

EVALUATING MARINE GAS-HYDRATE SYSTEMS PART I: STOCHASTIC ROCK-PHYSICS MODELS FOR ELECTRICAL RESISTIVITY AND SEISMIC VELOCITIES OF HYDRATE-BEARING SEDIMENTS

DIANA SAVA and BOB HARDAGE

Bureau of Economic Geology, Jackson School of Geosciences, The University of Texas at Austin, Austin, TX 78713, U.S.A. diana.sava@beg.utexas.edu

(Received June 12, 2010; revised version accepted September 1, 2010)

ABSTRACT

Sava, D. and Hardage, B.A., 2010. Evaluating marine gas-hydrate systems. Part I: Stochastic rock-physics models for electrical resistivity and seismic velocities of hydrate-bearing sediments. *Journal of Seismic Exploration*, 19: 371-386.

There is an increased need for investigating marine gas-hydrate systems to estimate the magnitude of the energy resource represented by the hydrate and to identify any unstable seafloor conditions that may result from hydrate dissociation, which can jeopardize drilling activities. Deep-water gas-hydrate systems can be studied on large scales with geophysical techniques, such as seismic and electrical surveys. To evaluate near-seafloor gas-hydrate environments we first need to build rock-physics quantitative relations between measurable parameters, such as elastic and electrical properties of sediments containing hydrates, and gas-hydrate saturation. In this study we assume a model of isotropic, load-bearing hydrates, uniformly distributed in the near-seafloor sediments. This Part I of a 2-paper series presents a method for stochastic joint modeling of elastic properties and electrical resistivity of gas-hydrate sediments. The petrophysical parameters involved in the modeling are difficult to estimate and are uncertain. Therefore, probability distribution functions (PDFs) are used to account for the uncertainty associated with each of the petrophysical quantities involved in the modeling. Both electrical resistivity and seismic velocities depend on porosity of the sediments and hydrate concentration, and we refer to them as common model parameters. A Monte Carlo procedure is used to draw values for these common parameters from their associated PDFs and then compute the corresponding velocity and electrical resistivity values using Monte Carlo draws from the PDFs for each of the petrophysical parameters that are required for elastic modeling and for Archie equation for electrical resistivity. The outcome of this procedure is represented by many Monte Carlo realizations that jointly relate hydrate concentration, resistivity, and seismic propagation velocity. This joint relation varies with depth and it is non-unique and uncertain due to variability of the input parameters. These theoretical relations can then be used to estimate hydrate concentration in Green Canyon Gulf of Mexico through a joint inversion technique presented in the Part II.

KEY WORDS: gas hydrates, rock-physics, elastic properties, modeling, Gulf of Mexico.

INTRODUCTION

Evidence is accumulating that numerous hydrate systems exist across many of the deep-water areas of the Gulf of Mexico. These deep-water systems need to be evaluated to determine the magnitude of the energy resource represented by the embedded hydrate and to identify unstable seafloor conditions that may be associated with hydrate dissociation. Local sampling (drilling, logging, and coring) is invaluable for evaluating deep-water hydrates, but such data cannot characterize volumetric distributions of hydrates. Remote-sensing techniques, such as seismic reflection profiling, must be combined with these in situ data to survey large areas where there is evidence of deep-water hydrates.

Gas hydrates increase both the elastic moduli and the electrical resistivity of the sediments in which they occur (Collett, 2001). Therefore, the most common data used to characterize hydrate systems are electrical resistivity and sonic and dipole-sonic logs acquired in wells, combined with remotely acquired seismic, electromagnetic, and direct-current data. The relation between hydrate concentration and resistivity of strata containing hydrates is non-unique and uncertain. Similarly, any relationship between hydrate concentration and seismic propagation velocity in sediment containing hydrate is also uncertain. Some of these sources of uncertainty are related to data-measurement errors, limited availability of data, inability to define accurate mineral fractions that exist in the sediment that host hydrate, inaccurate porosity information, poor understanding of how hydrate is distributed among sediment grains, unexpected spatial variability of rock properties, and inadequate understanding of numerous other physical conditions and processes associated with hydrate systems. Therefore, by combining quantitatively various types of hydrate-sensitive information, we can better constrain the predictions about gas hydrate distribution.

The modeling approach described in the paper combines rock-physics theories and empirical relations with stochastic simulations. We show examples from the Green Canyon area, Gulf of Mexico.

ELECTRICAL RESISTIVITY OF GAS-HYDRATE SYSTEMS IN MARINE ENVIRONMENTS

The host sediments of gas-hydrate systems in deep-water, near-seafloor environments are represented by highly unconsolidated, high-porosity, near-suspension-regime sediments. In these environments, sediment grains are loosely packed, and electrical current can flow freely through the conductive phase represented by brine. The electrical resistivity of such sediments is well characterized by the Hashin and Shtrikman (1962) lower bound on electrical

resistivity for composite materials (Mendelson and Cohen, 1982; Berryman, 1995; Wempe, 2000).

Gas hydrates increase the resistivity of sediments because hydrates are electrical insulators, as hydrocarbons are. Therefore, in principle, we can use the same techniques to estimate hydrate saturation as those used to estimate hydrocarbon saturation in the oil industry. The most common empirical technique used to determine hydrocarbon saturation is the Archie equation. This equation has been used to analyze resistivity responses of fluid-filled porous rocks and to determine their water saturation for more than six decades in the form (Archie, 1942),

$$R = aR_w\phi^{-m}S_w^{-n} \quad , \quad (1)$$

where R is the resistivity of the logged interval (ohm-m), a is a dimensionless parameter related to the grain shape of the sediments and the tortuosity of the pore space, R_w is the resistivity of the pore fluid (ohm-m), ϕ is the porosity of the sediments (dimensionless fraction), m is a dimensionless parameter related to the degree of consolidation and grain cementation, S_w is water saturation (dimensionless fraction), and n is the saturation exponent (also a dimensionless parameter). In typical oil and gas reservoir applications, the internal geometric parameter, a , is ~ 1.0 , $n \sim 2$, and the cementation exponent, m , usually ranges from 2.0 to 2.56. However, for deep-water, near-seafloor strata within the hydrate stability zone, the cementation exponent, m , has significantly lower values than it does in deeper reservoirs (Mendelson and Cohen, 1982).

For sediments close to the suspension regime, the empirical parameters in the Archie Equation (cementation exponent, m , and internal geometric parameter, a) can be calibrated using the Hashin-Shtrikman (1962) lower bound on electrical resistivity. For a two-component system represented by insulating mineral grains and conductive brine, the internal geometric parameter a , and the cementation exponent m , are given as follows [Berryman, 1995, eq. (25)]:

$$a = (3 - \phi)/2 \quad , \quad m = 1. \quad (2)$$

Therefore, for highly unconsolidated sediments with large porosities and small effective pressure as found in deep-water, near-seafloor strata, we should use significantly smaller values for the cementation exponent m (as low as 1) than we do for deeper hydrocarbon reservoirs. Small values for the cementation exponent for unconsolidated sediments have also been observed by other researchers who have studied marine sediments (Jackson et al., 1978; Mendelson and Cohen, 1982).

To estimate hydrate concentration in marine sediments from electrical resistivity measurements, we need to build a baseline that describes the

resistivity of 100% brine-saturated sediments as a function of depth across the hydrate stability zone. The electrical resistivity of marine sediments fully saturated with brine is derived using the Archie equation with S_w set to 1. Other parameters in the Archie equation, such as porosity of the sediments ϕ , resistivity of the brine R_w , cementation exponent m , and internal geometric parameter a , vary with depth. These depth-dependent variations need to be calibrated at each study site.

Porosity information for near-seafloor strata across the study area in Green Canyon is available from geotechnical borings. Fig. 1 presents laboratory-measured porosity data as a function of depth compiled from two study sites.

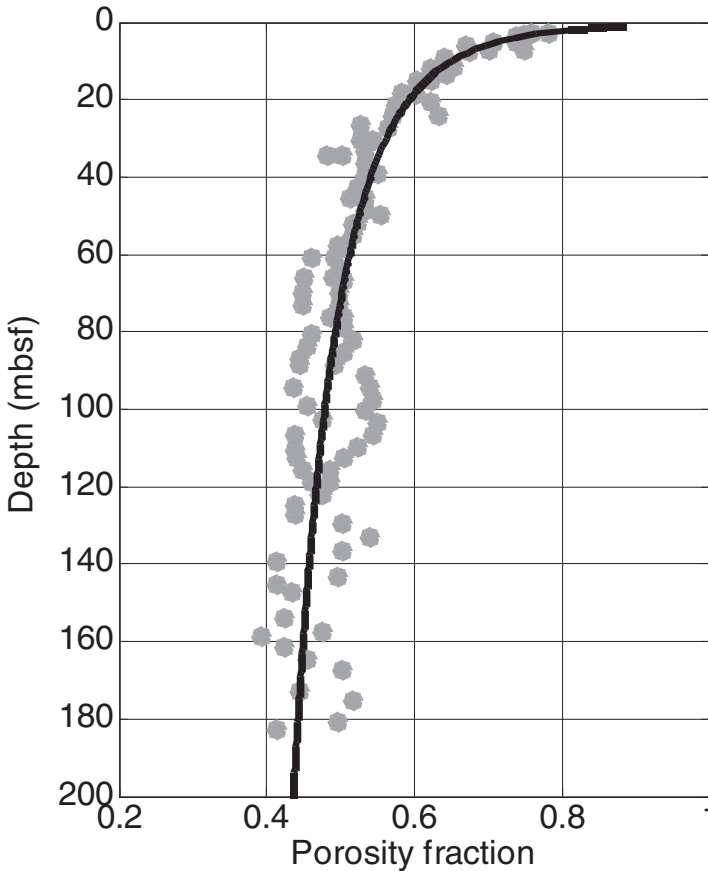


Fig. 1. Porosity fraction of sediments within an interval of the gas hydrate stability zone (GHSZ) as a function of depth below seafloor. The data are compiled from geotechnical borings collected by Chevron at two sites in Green Canyon, Gulf of Mexico. The superimposed curve is a non-linear, least-squares fit to the data.

The curve superimposed on the data from Fig. 1 is a non-linear least squares fit of the form:

$$\phi = \phi_0 \exp[-k \log(z)] \quad , \quad \text{with } z > 1 \text{ m.} \quad (3)$$

In eq. (3), ϕ represents the porosity of the sediments as a function of depth, and z is depth in meters below seafloor. The empirical parameters in eq. (3) are ϕ_0 (which represents the porosity of sediments 1 m below the seafloor) and k (which represents the decay rate of porosity with the logarithm of depth). For this data set, we used a non-linear, least-squares method to obtain a value of 0.887 for ϕ_0 and a value of 0.1343 m^{-1} for the decay constant k . The relations for porosity variation with depth due to compaction in previous published studies (Rubey and Hubbert, 1958; Allen and Allen, 1990; Ramm and Bjoerlykke, 1994) do not include such a logarithmic dependence on depth. However, previous empirical relations without the logarithm of depth cannot fit the porosity data from deep-water, near-seafloor strata in the Green Canyon, GOM. Porosity reduces more rapidly in the shallow sediments than in deeper sediments.

The cementation exponent m increases with depth due to the increasing degree of consolidation. Even though porosity decreases significantly within the first few tens of meters of seafloor sediment, the expected variation of the cementation exponent may not be as drastic. A study by Wempe (2000) shows that for sediments close to the suspension regime (with porosities greater than 40% and low effective pressures), there is a small variation in electrical resistivity when porosity decreases from 80% to 40%. The electrical resistivity of such sediments close to the suspension regime are well described by the Hashin-Shtrikman lower bound. In this analysis we assume that the cementation exponent m increases linearly with depth and effective pressure, as opposed to a non-linear variation with depth. The variation of the cementation exponent is determined such that the computed electrical resistivity for brine saturated sediments using Archie Equation qualitatively matches the observed background trend in the well logs, with the constraint that at seafloor, cementation exponent is equal to 1. This linear increase of cementation exponent with depth should be calibrated at each study site.

The internal geometric parameter, a , also increases with depth. For this parameter, eq. (2) shows its dependence on porosity when sediments are close to being in a suspension regime. The resistivity of brine R_w increases with depth because temperature increases according to the local geothermal gradient. Geotechnical measurements made on seafloor cores also provide information on formation salinity. Based on this information, and using the assumption of a normal geothermal gradient, we estimate the variation of brine resistivity with depth. The saturation exponent n does not enter into the computation of the baseline for brine-saturated sediments because $S_w = 1$ in this case.

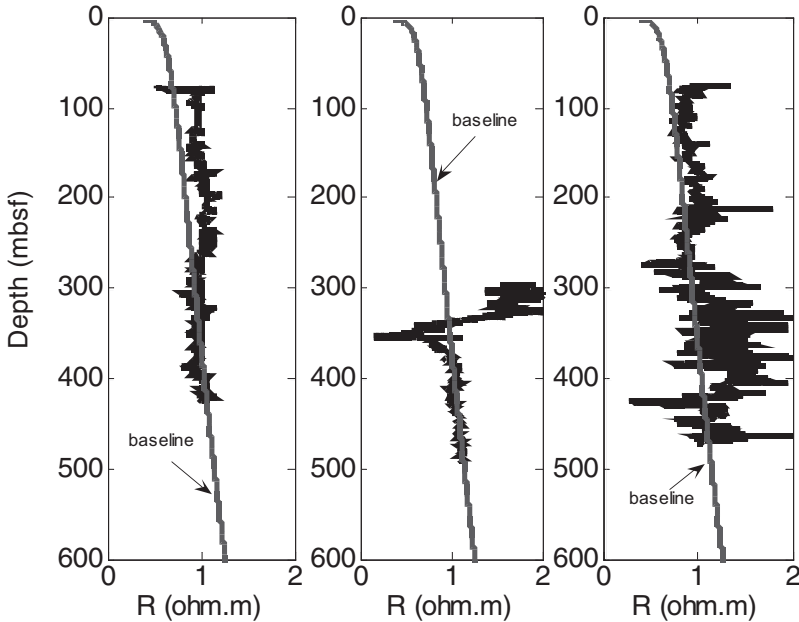


Fig. 2. Resistivity (R) log data for three randomly chosen wells in Green Canyon, GOM. Superimposed is the baseline for sediments fully saturated with brine. The cementation exponent m varies linearly from 1 at the seafloor to 1.7 at 600 m below seafloor. The internal geometrical factor a increases with decreasing porosity as in eq. (2).

Fig. 2 shows electrical resistivity logs for three different wells across Green Canyon, Gulf of Mexico. These measurements were performed while drilling. On each panel, we superimpose the baseline for resistivity of sediments that are fully saturated with brine, computed using the Archie equation and the depth variations of the Archie equation parameters described above. From this figure we observe that the baseline resistivity for 100% brine-saturated sediments is a good description of the background trend in all three wells. Long-wavelength deviations from the baselines to larger resistivity-log values are interpreted to be caused by the presence of hydrates or free gas in the pore space.

Using the calibrated parameters a and m in the Archie equation for unconsolidated sediments saturated with brine, hydrate concentration can be predicted using electrical resistivity log-data (R), porosity information (ϕ), and resistivity of the brine (R_w). The hydrate concentration in sediment pores can be estimated from the Archie equation as a function of the volumetric fraction of water saturation [S_w from eq. (1)]:

$$C_{GH} \equiv 1 - S_w = 1 - [(aR_w/R)\phi^{-m}]^{1/n} . \quad (4)$$

ELASTIC PROPERTIES OF GAS-HYDRATE SYSTEMS

Our goal of rock-physics elastic modeling of marine hydrate systems is to define quantitative relations between hydrate concentration in marine sediments and seismic measurements. Many published relations between hydrate concentration and seismic attributes are empirical (Pearson et al., 1983; Miller et al., 1991; Wood et al., 1994; Holbrook et al., 1996; Lee et al., 1996; Yuan et al., 1996; Collett, 1998; Lu and McMechan, 2002, 2004). Empirical approaches are easy to implement, but they do not have predictive power and should be used only at the specific site where the relationships are derived. An additional shortcoming is that empirical relations do not provide insights into the morphological character of how gas hydrates are distributed within sediments.

There are also studies that use physics-based, effective-medium models of hydrate systems to relate hydrate concentration to seismic properties (Helgerud et al., 1999; Ecker et al., 2000; Carcione and Tinivella, 2000; Chand et al., 2004; Winters et al., 2004; Waite et al., 2004; Kleinberg and Dai, 2005; Murray et al., 2006; Zillmer, 2006). Some of these effective-medium models are based on Dvorkin and Nur's (1996) model of unconsolidated sediments, which uses Hertz-Mindlin's contact theory (Mindlin, 1949; Mavko et al., 1998). These models for unconsolidated sediments have been applied successfully to deeper marine sediments (Prasad and Dvorkin, 2001), but they do not explain lab observations (Zimmer, 2003; Yun et al., 2005) and in-situ observations (Hardage et al., 2010) made within the first 200 meters below the seafloor where sediments have small shear strengths, large V_p/V_s ratio, and low effective pressure.

In this paper, we use models of hydrate systems applicable to the highly unconsolidated, low-effective-pressure zone that spans the first 200 or 300 meters of sub-seafloor strata (Sava and Hardage, 2006; 2010). The host sediments are modeled using the approach by Dvorkin and Nur (1996), with the distinction that the elastic properties of sediments at critical porosity (Nur et al., 1998) are described by Walton's smooth model (Walton, 1987), as opposed to the Hertz-Mindlin model (Mindlin, 1949; Mavko et al., 1998). Walton's theory seems particularly appropriate for highly unconsolidated sediments at low effective pressure, where grain rotation and slip along grain boundaries are likely to occur during compaction. Therefore, we assume that at critical porosity the effective elastic moduli of the dry-mineral frame of sediments can best be calculated by using Walton's smooth contact model for elastic particles.

The expressions for bulk and shear moduli of a random arrangement of dry spheres that resembles the unconsolidated dry sediments of near-seafloor strata at critical porosity are (Walton, 1987):

$$K_{\text{eff}} = \sqrt[3]{\{[C^2(1 - \phi_c)^2 G^2]/[18\pi^2(1 - \nu)^2]P\}} \quad , \quad (5)$$

$$G_{\text{eff}} = (3/5)K_{\text{eff}} \quad . \quad (6)$$

In eqs. (5) and (6), K_{eff} and G_{eff} are the effective bulk and shear moduli, respectively, for the granular material. C is the coordination number, which represents the average number of contacts between a grain and its neighboring grains. ϕ_c is the critical porosity of the sediments, G is the shear modulus of the mineral grains, ν is the Poisson's ratio of the mineral grains, and P is the effective pressure, taken here as the simple difference $P_{\text{tot}} - P_{\text{fld}}$.

For porosity values smaller than critical porosity, the elastic properties of the dry-mineral frame are estimated using the modified Hashin-Shtrikman lower bound (Hashin and Shtrikman, 1963; Dvorkin and Nur, 1996). For porosity values larger than critical porosity we use a modified Hashin-Shtrikman (1963) upper bound to derive the elastic properties of the dry-mineral frame of granular materials (Dvorkin et al., 1999). Gassmann's (1951) theory is then used to derive the density and bulk and shear moduli of the sediments saturated with various fluids.

The model for unconsolidated sediments described above is used to derive the depth-dependent baseline, across the gas hydrate stability zone, for elastic properties of sediments that are 100% saturated with brine.

The porosity variation with depth was discussed in the previous section. The effective pressure as a function of depth is derived assuming hydrostatic pore pressure, and total pressure increasing according to the density. The coordination number increases with depth because of increasing effective pressure and decreasing porosity. In this study we relate the coordination number linearly to effective pressure and depth rather than to porosity. At the seafloor, the coordination number is 1, and it increases linearly with depth so that at 600 m below the seafloor, it has a value of 6.7. Any calibration of the coordination number is site specific.

We assume that the density and the elastic moduli for the mineral grains are those corresponding to Gulf of Mexico clays (Mavko et al., 1998) because geotechnical borings indicate clays are the dominant minerals. The brine density and bulk modulus are derived as a function of pressure and temperature using Batzle and Wang (1992) empirical relations, assuming a brine salinity of 59000 ppm from geotechnical data.

Using this model for unconsolidated sediments and the assumptions discussed above, we derive the baseline for P-wave velocities of brine saturated sediments as a function of depth.

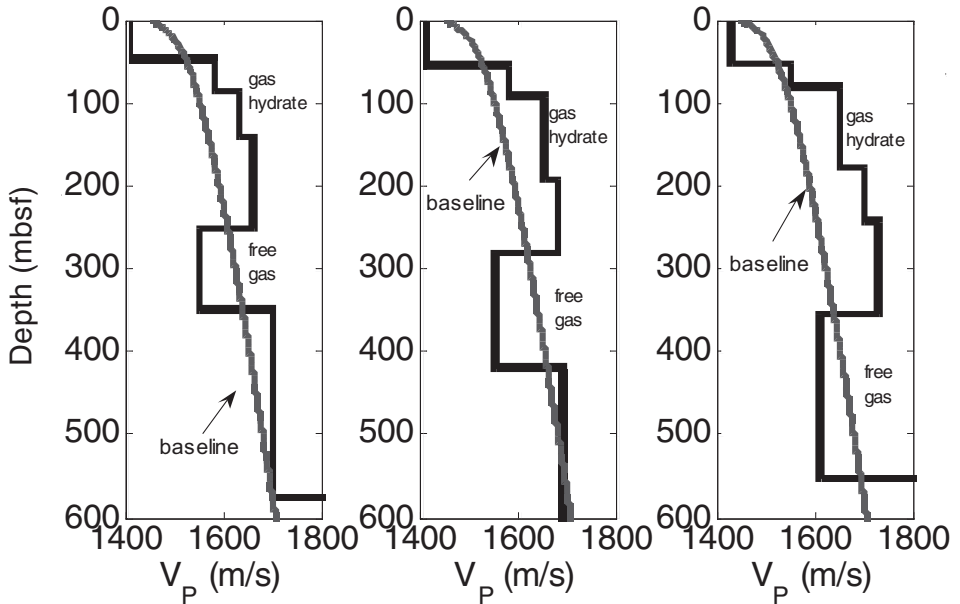


Fig. 3. Seismic P-wave interval velocities, as a function of depth below seafloor, estimated at three different well locations. Superimposed are baselines for brine-saturated sediments with 95% clay minerals and 5% quartz.

Fig. 3 presents seismic P-wave interval velocities determined using a raytrace-based velocity analysis technique (DeAngelo et al., 2008) at different well locations. Superimposed on these seismic velocities is the computed baseline for P-wave velocities as a function of depth for sediments saturated with brine (the same baseline for all three cases). Intervals with higher P-wave velocities than the baseline occur within the hydrate stability zone at all three well-locations. These intervals are likely hydrate-bearing. In each of the examples from the three panels in Fig. 3, there is an interval with lower velocity below the higher-velocity interval, which appears to correspond to free gas below the hydrate stability zone. In Fig. 3, the baseline velocities assumes a mineralogy with an average of 95% clay, the rest of 5% being represented by quartz.

Once the elastic properties of the host sediments as a function of depth are derived, hydrates are introduced into the system to derive the quantitative relation between seismic velocities and hydrate concentration. Hydrates can occur in various morphologies in relation to their host sediments (Sava and Hardage, 2006; 2010), for example disseminated (load-bearing or floating in the pores), layered (horizontally or vertically), or massive. In this paper we assume the model for disseminated, load-bearing hydrates because laboratory

observations (Yun et al., 2005; Winters et. al, 2004) indicate this option may be the most likely model for hydrate distribution in marine sediments.

FORWARD MODELING AND MONTE CARLO SIMULATIONS OF C_{GH} -R- V_p JOINT RELATION

In this section we discuss the forward modeling problem for which we use the Archie equation and the rock-physics elastic model described in previous sections. The outcome of the forward modeling is a joint theoretical relation between hydrate concentration, electrical resistivity, and velocity of sediments containing hydrates. Based on this joint theoretical relation calibrated for our study area in Green Canyon, Gulf of Mexico, we can then estimate hydrate concentrations using actual measurements of electrical resistivity-log and seismic velocity (Part II).

Both electrical resistivity and elastic properties of hydrate-bearing sediments depend on sediment porosity (ϕ) and hydrate concentration (C_{GH}) in pores. They also depend on the volumetric fraction of clay minerals (V_{cl}), when the resistivity of clays is significantly lower than that of the other mineral grains. The volumetric fraction of clay minerals can be estimated from gamma-ray logs. Therefore, we can model the joint relation between hydrate concentration, resistivity and velocities using the Archie equation or a form of it modified for clay volume, and the rock physics elastic model for unconsolidated sediments with load-bearing hydrates.

Any theoretical relation linking hydrate concentration, resistivity, and velocity is non-unique and uncertain. The uncertainty is caused by the fact that the parameters needed in the modeling, such as porosity, cementation exponent, geometric factor, resistivity of brine, saturation exponent, elastic properties of mineral, brine, and hydrates, volumetric fraction of clay minerals, effective pressure, critical porosity, and coordination number do not have fixed values, but are themselves uncertain and variable. Thus, each parameter in the rock-physics elastic modeling, and in the Archie equation (with a clay term), is expressed as a probability distribution function (PDF). The PDFs used in the modeling are either Gaussian distributions or uniform distributions. Gaussian distributions are used for parameters whose expected values can be calibrated or measured. The mean of the Gaussian function is the expected value of the parameter, and the standard deviation defines the uncertainty associated with this expected parameter value. These expected values for parameters such as cementation exponent, geometric factor, resistivity of brine, volumetric fraction of clay, elastic properties of brine, coordination number, and effective pressure vary with depth, as discussed in previous sections. Therefore, their individual PDFs vary with depth. The standard deviation for these parameters is assumed to be 5%, and does not vary with depth. Other parameters described by

Gaussian distributions are the elastic moduli and density of mineral grains, whose expected values are assumed from published laboratory results (Mavko et. al, 1998). The PDFs for the elastic properties of the mineral grains do not change with depth, and their standard deviation is assumed to be also 5%. The mean values used for the mineral grains are displayed in Table 1.

Table 1. Mean values for elastic moduli and density of clay and quartz minerals.

K_{clay} (GPa)	G_{clay} (GPa)	ϕ_{clay} (g/cm ³)	K_{quartz} (GPa)	G_{quartz} (GPa)	ϕ_{quartz} (g/cm ³)
25	9	2.55	37	44	2.65

In contrast to a Gaussian distribution, a uniform distribution is used when the range of variability for a certain model parameter can be defined. A uniform distribution assumes that within the range of variability being considered, any value of the described parameter is equally probable. Uniform distributions are used for the saturation exponent n , needed in the Archie equation, resistivities of clay minerals, critical porosity, elastic moduli and density of hydrates, and hydrate concentration. These parameters and their associated PDF do not vary with depth. The range of variability for the model parameters with uniform distributions are given in Table 2.

Table 2. Range of variability for parameters with uniform distribution: saturation exponent in Archie Equation (n), Resistivity of clay minerals (R_{clay}), critical porosity (ϕ_{critic}), bulk moduli of gas-hydrate (K_{GH}), shear modulus of gas-hydrate (G_{GH}), and density of gas-hydrate (ρ_{GH}). The values for moduli and density of hydrates are taken from Sloan and Koh (2008).

n	R_{clay} (ohm.m)	ϕ_{critic} (%)	K_{GH} (GPa)	G_{GH} (GPa)	ρ_{GH} (g/cm ³)
1.7-2.3	20-1000	75%-85%	6-8.7	2.4-3.6	0.90-0.94

The PDFs are assumed to be mutually independent. For example, the PDFs for the elastic moduli are not coupled together, and the Monte Carlo draws for K and G might yield a high value for K and a low value for G , even though this implies an unlikely mineralogy and/or microstructure. As a result, the joint PDFs might be broader than they would be if the PDFs were mutually dependent. However, the range of variability assumed for the elastic moduli of the minerals and gas-hydrates used in the modeling is small, within the limits

encountered by various authors when studying Gulf of Mexico clays (Mavko et al., 1998) and gas-hydrates (Sloan and Koh, 2008).

The parameters involved in both the rock physics elastic modeling and the Archie equation (modified for clay) are denoted as common parameters. There are three of these common parameters: porosity (ϕ), hydrate concentration (C_{GH}), and volumetric fraction of clay (V_{cl}). A Monte Carlo procedure is used to draw values for these common parameters from their associated PDFs and then compute the corresponding velocity and resistivity values using Monte Carlo draws from the PDFs for each of the petrophysical parameters that are required for elastic modeling and for Archie equation. In this fashion we obtain many Monte Carlo realizations that jointly relate hydrate concentration, resistivity, and seismic propagation velocity. This joint relation is non-unique and uncertain due to variability of the input parameters and varies with depth. The theoretical relation of hydrate concentration, electrical resistivity, and velocity can be expressed mathematically as a probability distribution function in a three-dimensional model space (C_{GH} , V_p , R). This model space is updated with depth.

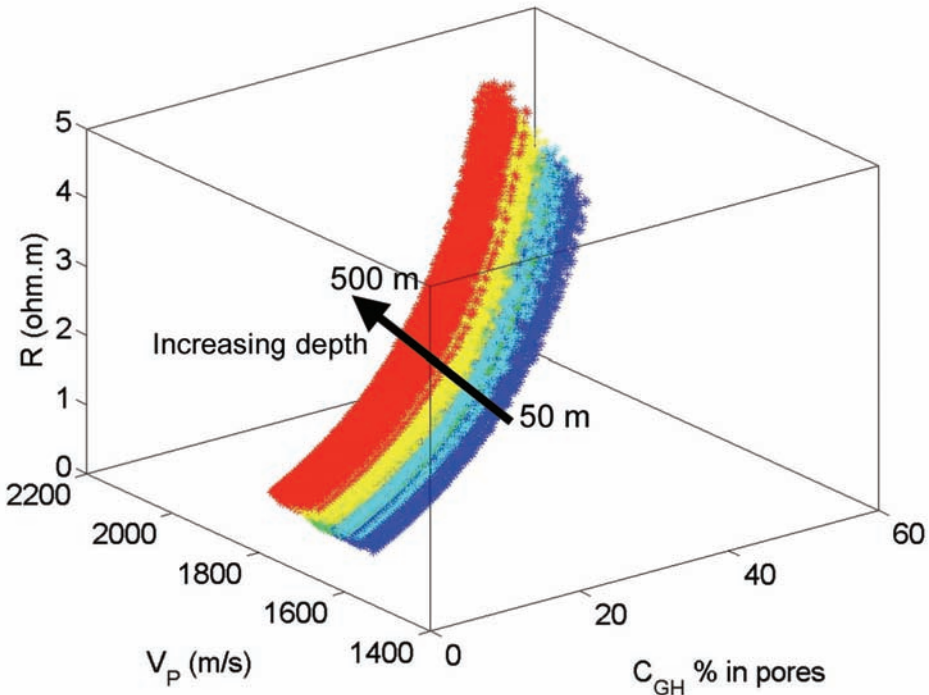


Fig. 4. Monte Carlo simulations for the joint theoretical relation between hydrate concentration (C_{GH}), P-wave velocity (V_p), and resistivity (R). Data are color-coded by depth. The arrow indicates increasing depth over the gas hydrate stability zone. Gas hydrate is assumed to be disseminated and load-bearing.

Based on these Monte Carlo realizations, we derive at each depth-step a joint theoretical PDF for hydrate concentration, P-wave velocity, and resistivity, generically denoted as $\xi(C_{GH}, V_p, R)$. This PDF represents mathematically the quantitative relations between hydrate concentration, P-wave velocity and electrical resistivity with their inherent uncertainty.

Fig. 4 presents the results for Monte Carlo simulations of the joint theoretical relation between hydrate concentration, P-wave velocity, and resistivity. The data are color-coded by depth, and the arrow indicates increasing depth within the gas hydrate stability zone (GHSZ). As expected, both electrical resistivity and P-wave velocity increase with increasing hydrate concentration and with increasing depth. At a fixed depth, the scatter in the data is caused by the uncertainty in the input parameters used in the elastic rock-physics model and Archie equation.

Based on these theoretical relations expressed as PDFs, calibrated for our study area in Green Canyon Gulf of Mexico, we can estimate the in-situ hydrate concentration using the actual measurements on electrical resistivity in wells and seismic velocity at well locations, as presented in Part II.

CONCLUSIONS

We have derived rock-physics joint theoretical relations between hydrate concentration, seismic velocity, and electrical resistivity for sediments from a deep-water of Green Canyon, Gulf of Mexico. These quantitative relations are uncertain because the parameters involved in both rock-physics elastic model and Archie Equation for electrical resistivity cannot be estimated exactly. We account for this uncertainty by using probability distribution functions (PDF) for each of the modeling parameters as a function of depth. One of the key petrophysical parameter that affects both elastic and electrical resistivity of sediments with hydrates is porosity. We derived a new porosity variation with depth for the deep-water near-surface sediments from geotechnical data in Green Canyon.

Both electrical resistivity and elastic properties of hydrate-bearing sediments depend not only on sediment porosity (ϕ), but also on hydrate concentration (C_{GH}) in pores. A Monte Carlo procedure is used to draw values for these common parameters from their associated PDFs and then compute the corresponding velocity and electrical resistivity values using Monte Carlo draws from the PDFs for each of the petrophysical parameters that are required for elastic modeling and for Archie equation. In this way we obtain many Monte Carlo realizations that jointly relate hydrate concentration, electrical resistivity, and seismic propagation velocity as a function of depth. Based on these joint theoretical relations we can then estimate hydrate concentration using the joint inversion technique presented in Part II.

ACKNOWLEDGEMENTS

Research funding was provided by the U.S. Department of Energy (DOE/NETL Contract DE-PS26-05NT42405) and by the Minerals Management Service (Contract MMS 0105CT39388). Manuscript published with the approval of the director of the Bureau of Economic Geology.

REFERENCES

- Allen, P. and Allen, J., 1990. Basin Analysis: Principles and applications. Blackwell Scientific Publications, Oxford.
- Archie, G.E., 1942. The electric resistivity log as an aid in determining some reservoir characteristics. *Trans. AIME*, 46: 54.
- Batzle, M. and Wang, Z., 1992. Seismic properties of pore fluids. *Geophysics*, 57: 1396-1408.
- Bayes, T., 1783. An essay towards solving a problem in the doctrine of chances, *Phil. Trans. Roy. Soc.*, 53: 370-418.
- Berryman, J.G., 1995. Mixture theories for rock properties. In: Ahrens, U.J. (Ed.), *Rock Physics and Phase Relations: A Handbook of Physical Constants*. AGU, Washington, D.C.: 205-228.
- Carcione, J.M. and Tinivella, U., 2000. Bottom-simulating reflectors: Seismic velocities and AVO effects. *Geophysics*, 65: 54-67.
- Chand, S., Minshull, T.A., Gei, D. and Carcione, J.M., 2004. Elastic velocity models for gas-hydrate-bearing sediments-a comparison. *Geophys. J. Int.*, 159: 573-590.
- Clavier, C., Coates, G. and Dumanoir, J., 1977. The Theoretical and Experimental Bases for the "Dual Water" Model for the Interpretation of Shaly Sands. *SPE 6859*: 1-16.
- Collett, T.S., 1998. Well log evaluation of gas hydrate saturations. *Transact. Soc. Profess. Well Log Analysts*, 39th Ann. Logging Symp., Paper MM.
- Collett, T.S. (2001), A review of well-log analysis techniques used to assess gas-hydrate-bearing reservoirs. In: *Natural Gas Hydrates: Occurrence, Distribution, and Detection*. AGU *Geophys. Monograph*, 124: 189-210.
- DeAngelo, M.V., Murray, P.E., Hardage, B.A. and Remington, R.L., 2008. Integrated 2D 4-C OBC seismic velocity analysis of near-seafloor sediments, Green Canyon, Gulf of Mexico. *Geophysics*, 73: B109-B115.
- Dvorkin, J. and Nur, A., 1996. Elasticity of high-porosity sandstones: theory for two North Sea data sets. *Geophysics*, 61: 1363-1370.
- Dvorkin, J., Prasad, M., Sakai, A. and Lavoie, D., 1999. Elasticity of marine sediments. *Geophys. Res. Lett.*, 26: 1781-1784.
- Ecker, C., Dvorkin, J. and Nur, A., 2000. Estimating the amount of gas hydrate and free gas from marine seismic data. *Geophysics*, 62: 565-573.
- Gassmann, F., 1951. On the elasticity of porous media. *Vier. Natur. Gesellsch. Zürich*, 96: 1-23.
- Hardage, B.A., Roberts, H.H., Murray, P.E., Remington, R., Sava, D.C., Shedd W. and Hunt, J.Jr., 2010. Multicomponent seismic technology assessment of fluid-gas explosion geology, Gulf of Mexico. In: Collett, T., Johnson, A., Knapp, C. and Boswell, R. (Eds.), *Natural Gas Hydrates: Energy Resource Potential and Associated Geologic Hazards*. AAPG *Memoir* 89: 247-265.
- Hashin, Z. and Shtrikman, S., 1962. A variational approach to the theory of effective magnetic permeability of multiphase materials. *J. Appl. Phys.*, 33: 3125-3131.
- Hashin, Z. and Shtrikman, S., 1963. A variational approach to the elastic behavior of multiphase materials. *J. Mech. Phys. Solids*, 11: 127-140.
- Helgerud, M.B., Dvorkin, J., Nur, A., Sakai, A. and Collet, T., 1999. Elastic-wave velocity in marine sediments with gas hydrates: Effective medium modeling. *Geophys. Res. Lett.*, 26: 2021-2024.

- Holbrook, W.S., Hoskins, H., Wood, W.T., Stephen, R.A. and Lizarralde, D. & Leg 164 Scientific Party, 1996. Methane hydrate and free gas on the Blake Ridge from vertical seismic profiling. *Science*, 273: 1840-1843.
- Jackson, P.D., Taylor Smith, D. and Stanford, P.N., 1978. Resistivity-porosity-particle shape relationships for marine sands. *Geophysics*, 43: 1250.
- Kleinberg, R.L. and Dai, J., 2005. Estimation of the mechanical properties of natural gas hydrate deposits from petrophysical measurement. OTC, 17205, Offshore Technol. Conf., Houston, TX, May 2005.
- Lee, M.W., Hutchinson, D.R., Collet, T.S. and Dillon, W.P., 1996. Seismic velocities for hydrate bearing sediments using weighted equation. *J. Geophys. Res.*, 101: 347-358.
- Lu, S. and McMechan, G.A., 2002. Estimation of gas hydrate and free gas saturation, concentration, and distribution from seismic data. *Geophysics*, 67: 582-593.
- Lu, S. and McMechan, G.A., 2004. Elastic impedance inversion of multichannel seismic data from unconsolidated sediments containing gas hydrate and free gas. *Geophysics*, 69: 164-179.
- Mavko G., Mukerji, T. and Dvorkin, J., 1998. *The Rock Physics Handbook*. Cambridge University Press, Cambridge.
- Mendelson, K.S. and Cohen, M.H., 1982. The effect of grain anisotropy on the electrical properties of sedimentary rocks. *Geophysics*, 47: 257-263.
- Miller, J.J., Lee, M.W. and von Huene, R., 1991. An analysis of seismic reflection from the base of a gas hydrate zone, offshore Peru. *AAPG Bulletin*, 75: 910-924.
- Mindlin, R.D., 1949. Compliance of elastic bodies in contact. *J. Appl. Mech.*, 16: 259-268.
- Murray, D.R., Kleinberg, R.L., Sinha, B.K., Fukuhara, M., Osawa, O., Endo, T. and Namikawa, T., 2006. Saturation, acoustic properties, growth habit, and state of stress of a gas hydrate reservoir from well logs. *Petrophysics*, 47: 129-137.
- Nur, A., Mavko, G., Dvorkin, J. and Galmudi, D., 1998. Critical porosity: a key to relating physical properties to porosity in rocks. *The Leading Edge*, 17: 357-362.
- Pearson, C.F., Hallek, P.M., McGuire, P.L., Hermes, R. and Mathews, M., 1983. Natural gas hydrate deposits: a review of in-situ properties. *J. Phys. Chem.*, 87: 4180-4185.
- Prasad, M. and Dvorkin, J., 2001. Velocity to porosity transform in marine sediments. *Petrophys.*, 42: 429-437.
- Ramm, M. and Bjoerlykke, K., 1994. Porosity/depth trends in reservoir sandstones: assessing the quantitative effects of varying pore-pressure, temperature history and mineralogy, Norwegian shelf data. *Clay Miner.*, 29: 475-490.
- Rubey, W. and Hubbert, M.K., 1959. Role of fluid pressure in mechanics of overthrust faulting, II. *Geol. Soc. Amer. Bull.*, 70: 167-206.
- Sava, D.C. and Hardage, B.A., 2006. Rock physics characterization of hydrate-bearing deepwater sediments. *The Leading Edge*, 25: 616-619.
- Sava, D.C. and Hardage, B.A., 2010. Rock-physics models for gas-hydrate systems associated with unconsolidated marine sediments. In: Collett, T., Johnson, A., Knapp, C. and Boswell, R. (Eds.), *Natural Gas Hydrates: Energy Resource Potential and Associated Geologic Hazards*. AAPG Memoir 89: 505-524.
- Sloan, D.E. and Koh, C.A., 2008. *Clathrate Hydrates of Natural Gases*, 3rd Ed., CRC Press, Boca Raton.
- Walton, K., 1987. The effective elastic moduli of a random packing of spheres, *J. Mech. Phys. Solids*, 35: 213-226.
- Waite, W.F., Winters, W.J. and Mason, D.H., 2004. Methane hydrate formation in partially water-saturated Ottawa sand. *Am. Mineral.*, 89: 1202-1207.
- Wempe, W., 2000. *Predicting Flow Properties Using Geophysical Data - Improving Aquifer Characterization*. Ph.D. thesis, Stanford University.
- Winters, W.J., Pecher, I.A., Waite, W.F. and Mason, D.H., 2004. Physical properties and rock-physics models of sediment containing natural and laboratory-formed methane gas hydrate. *Am. Mineral.*, 89: 1221-1227.
- Wood, W.T., Stoffa, P.L. and Shipley, T.H., 1994. Quantitative detection of methane hydrate through high-resolution seismic velocity analysis. *J. Geophys. Res.*, 99: 9681-9695.

- Yuan, T.S., Hyndman, G.D., Spence, G.D. and Desmons, B., 1996. Seismic velocity increase and deep-sea gas hydrate concentration above a bottom-simulating reflector on the northern Cascadia continental slope. *J. Geophys. Res.*, 101: 13655-13671.
- Yun, T.S., Francisca, F.M., Santamarina, J.C. and Ruppel, C., 2005. Compressional and shear wave velocities in uncemented sediment containing gas hydrate. *Geophys. Res. Lett.*, 32: L10609-L10613.
- Zillmer, M., 2006. A method for determining gas-hydrate or free-gas saturation of porous media from seismic measurements. *Geophysics*, 71: N21-N32.
- Zimmer, M.A., 2003. Controls on the Seismic Velocities of Unconsolidated Sands: Measurements of Pressure, Porosity and Compaction Effects. Ph.D. thesis, Stanford University.

SUBJECT INDEX, Volume 19, 2010

- absorbing boundary conditions 1, 2, 9, 18, 19, 37, 122, 130, 175, 185, 186
- absorption 1, 2, 4, 9, 12, 13, 18, 104, 119, 185
- acoustic modeling 19, 174, 182, 185
- adaptive mesh refinement 122-124, 127, 135, 136
- aliasing 280, 282-284, 290, 295-297, 299, 301, 322, 340, 343
- anisotropy 3-5, 19, 22, 23, 32, 37, 40, 44, 45, 53, 58, 64-69, 188, 189, 200, 202, 203, 223-225, 227, 349, 350, 354, 356, 358, 359, 364, 365, 370, 371, 385
- azimuthal anisotropy 188, 189, 200, 202

- basis pursuit 304, 307, 320
- Biot/squirt mechanism 1, 4, 19
- boundary conditions 1-3, 9, 14, 15, 18, 19, 22, 37, 122, 130, 175, 185, 186, 208, 227
- Bowers equation 142, 150-152, 154, 157

- carbonate reservoir 65, 86, 142
- channel analysis 162, 163
- conjugate gradients 321, 322, 326, 329, 335, 345, 346, 348
- crack density 43-48, 51-54, 57-65, 67

- damped least-squares 322
- data regularization 321, 322
- deep-water 264, 371-373, 375, 383
- density 4, 8, 24, 28, 43-49, 51-55, 57-65, 67, 78, 79, 85, 89, 128, 130, 142, 143-145, 150, 152, 153, 157, 176, 178, 210, 232, 235, 236, 237-242, 244-247, 249, 251-253, 255, 256, 273, 284, 285, 378, 381
- difference image 280, 292
- dipole sonic logs 87, 88, 92, 96, 99-102, 236

- effective pressure 142, 143, 150-154, 157, 373, 375, 377, 378, 380, 381
- elastic properties 45, 47, 50, 56, 58, 59, 66-69, 237, 350, 371, 377, 378, 379-381, 383
- elastic tensor 44, 58
- EMD 161-166, 169-172
- error function 249, 253, 254, 257, 259-262

- finite-difference 1, 3, 6, 7, 18, 19, 22, 23, 40, 41, 69, 136, 174, 176, 177, 178, 185, 186, 208-214, 216, 218, 220-222, 225, 226, 282, 283, 284, 286
- fluids 5, 40, 70, 72, 79, 85, 141, 378, 384
- fractured 45-48, 67-70, 72, 76, 86, 371

- gas hydrates 271, 279, 371-373, 377, 384, 385
 Gaussian 70, 73, 75, 76, 85, 146, 147, 178, 240, 249-251, 253, 255, 256, 257-261, 273, 326, 380, 381
 Gaussian kernel function 70
 geological pattern 304
 geostatistics 142, 159
 Gulf of Mexico 264, 265, 279, 371, 372, 374, 376, 378, 380, 382-384
- heavy oil 88, 96, 100-102, 158, 231, 232, 236, 248
 high-resolution algorithm 122
 hydrate 263-266, 269, 271-279, 371-374, 376-386
- image ray 187, 188, 192-194, 197, 205
 instantaneous frequency 161-171, 238, 241
 internal multiples 103-109, 111, 114, 117, 120, 131
 interpolation 24-26, 41, 42, 145, 148, 302, 308, 322, 323, 336, 347, 348
 inverse scattering 103-105, 117, 120, 121
 inversion 44, 45, 57, 65, 78, 104-106, 120-122, 143, 158, 203, 208, 226, 232, 235, 238-241, 247, 264, 265, 271-275, 277, 278, 304, 305-307, 311-313, 315, 320, 321, 324, 327, 332, 322, 323, 326, 329, 335, 347, 348, 370, 371, 384, 385
- kriging 87, 88, 101, 102, 142, 145-148, 154, 155
- linearized methods 349, 350
- matching pursuit 85, 86, 304, 306-309, 311, 320, 321
 modeling 1-4, 9, 10, 18, 19, 40, 41, 44, 45, 67, 68, 110, 121, 122, 134, 135, 160, 174-178, 182, 185, 186, 209, 226, 227, 273, 277, 279, 284, 287, 297, 301, 302, 321, 348, 349, 367, 371, 372, 377, 380, 382-385
 modified NAD algorithm 21, 22, 24
 multi-azimuth surveys 188
- nearly perfectly matched layer 174, 175, 185
 neural network 102, 231, 232, 238, 240, 241, 245, 247, 248
 NMO ellipse 188, 189, 194, 198, 205, 206
 NMO-stretch effect 280, 295, 298, 299, 301
 numerical dispersion 21-24, 26-29, 31-34, 40, 122, 131, 133, 208-210, 215, 217, 218, 221-223, 225, 226
 numerical modeling 1-3, 9, 19, 122, 135, 175, 176, 227
 Nyquist sampling theorem 280, 282-284
- ocean-bottom-cable 264
- P-P 264, 265, 267-271, 277, 278
 P-SV 19, 41, 186, 264, 265, 267-270, 277, 278
 pore pressure prediction 141-145, 148, 156, 157, 159, 160
 poroelastic media 1, 3, 9, 17, 19, 185, 186, 227
 probability density 249, 251-253, 273

random heterogeneous media 280-282, 284, 299, 302
 ray tracing 194, 198, 350-352, 361, 363, 364, 367-369, 371
 reflectivity 87-90, 92-96, 98, 99, 102, 239, 241, 242, 265, 267, 279, 304, 305-307,
 311-313, 315, 321, 327
 regularization 304-306, 327, 321-324, 329, 338, 343-345, 347, 348
 rock-physics 273, 371, 372, 377, 380, 383, 385, 386

 sandstone reservoir 70
 scattering 55, 66, 68, 103-105, 117, 120, 121, 224, 225, 280-282, 284, 287, 290,
 293, 295, 300-302
 sign-bit data 249, 250
 sparse spike inversion 304
 spatial sampling 23, 28, 280, 282-285, 288-291, 295-297, 299-302, 323
 spectral attenuation 70, 72, 85
 stacking velocity 141, 142, 144, 145, 148, 158
 staggered-grid 1, 3, 6, 7, 18, 19, 23, 174, 176-178, 186

 thickness variation 161-163, 166, 168, 170, 171
 thin bed 87, 161, 162, 168-171, 308
 time migration 141, 144, 145, 187-189, 192-198, 200, 202, 203, 205, 206, 235, 302
 time-lapse 280, 300, 302
 transmission losses 104, 106, 110, 111, 113, 115-117, 120
 travel times 122, 271, 349, 350, 366-370
 truncation artifact 280, 296, 297, 299, 301
 TTI media 208-211, 215-224, 226

 unsplit convolutional perfectly matched layer 19, 174, 175, 185

 variance 145, 249, 252, 256
 variography 142, 145, 146
 velocity analysis 142, 144, 148, 187-189, 195, 197, 201, 203, 271, 276, 279, 338,
 379, 384, 386
 V_p/V_s 67, 87, 88, 96, 99-103, 231, 232, 235-248, 264, 269, 271, 377

 wave equation redatum 322
 wave equation statics 322
 wave propagation 1, 3, 5, 9, 17-19, 21-23, 26, 40, 41, 67, 69, 121-124, 128-130,
 133-139, 174, 176, 178-181, 185, 186, 208, 209-211, 215, 216, 222,
 223, 226, 227, 281, 301, 302, 323, 341, 349, 350, 352
 wavefield simulation 22, 32, 41, 208, 225
 wavelets 71, 87, 88, 91, 92, 95, 96, 99, 101-103, 123, 136, 287, 295, 296, 320
 weighted-averaging 208-219, 221-223, 226, 229
 weighting coefficients 208, 211-218
 Wigner-Ville distribution 70, 71, 86

JOURNAL OF SEISMIC EXPLORATION

Volume 19

2010

CONTENTS

Number 1, January 2010

J. Chen, R.P. Bording, E. Liu Z. Zhang and J. Badal	The application of the nearly optimal sponge boundary conditions for seismic wave propagation in poroelastic media	1
D. Yang, G. Song and J. Zhang	A modified NAD algorithm with minimum numerical dispersion for simulation of anisotropic wave propagation	21
Y. Hu and G.A. McMechan	Theoretical elastic stiffness tensor models at high crack density	43
X. Wu And T. Liu	Analysis of seismic spectral attenuation based on Wigner-Ville distribution for sandstone reservoir characterization - a case study from West Sichuan Depression, China	69
L.R. Lines, P.F. Daley and L. Ibna-Hamid	The accuracy of dipole sonic logs and its implication for seismic interpretation	87

Number 2, April 2010

- J.E.M. Lira, K.A. Innanen,
A.B. Weglein and
A.C. Ramirez Correction of primary amplitudes
for plane-wave transmission loss
through an acoustic or absorptive
overburden with the inverse
scattering series internal multiple
attenuation algorithm: an initial
study and 1D numerical examples . 103
- T. Mi, J. Ma, H. Chauris
and H. Yang Multilevel adaptive mesh modeling
for wave propagation in layered
media 121
- E. Nosrat, A. Javaherian,
M.R. Torabi and H.B. Asiri Pore pressure prediction using
3D seismic velocity data: a case
study, a carbonate oil field,
SW Iran 141
- Y. Zhou, W. Chen, J. Gao
and Y. He Empirical mode decomposition
based instantaneous frequency
and seismic thin-bed analysis 161
- J. Chen, C. Zhang
and R.P. Bording Comparison between the nearly
perfectly matched layer and
unsplit convolutional perfectly
matched layer methods using
acoustic wave modeling 173
- W. Söllner, I. Tsvankin
and E. Filpo Ferreira da Silva Multi-azimuth prestack time
migration for anisotropic, weakly
heterogeneous media 187

Number 3, July 2010

- G. Wu, K. Liang and X. Yin Frequency-domain weighted
-averaging finite-difference
numerical simulation of qP wave
propagation in TTI media 207
- C.C. Dumitrescu and L. Lines Integrated characterization of
heavy oil reservoir using V_p/V_s
ratio and neural network analysis . 231

L.M. Houston, G.A. Glass and A.D. Dymnikov	Sign-bit amplitude recovery in Gaussian noise	249
M.V. DeAngelo, D.C. Sava, B.A. Hardage and P.E. Murray	Integrated 2D 4-C OBC analysis for estimating hydrate concentra- tions, Green Canyon, Gulf of Mexico	263
J. Matsushima and O. Nishizawa	Difference image of seismic reflection sections with highly dense spatial sampling in random heterogeneous media	279

Number 4, October 2010

T. Nguyen and J. Castagna	High-resolution reflectivity inversion	303
D.R. Smith, M.K. Sen and R.J. Ferguson	Data regularization and datuming by conjugate gradients	321
P.F. Daley, E.S. Krebes and L.R. Lines	Travel times in TI media: a comparison of exact, approximate and linearized methods	349
D. Sava and B.A. Hardage	Evaluating marine gas-hydrate systems. Part I: Stochastic rock-physics models for electrical resistivity and seismic velocities of hydrate- bearing sediments	371
	Subject Index Vol. 19, 2010	387
	Contents Vol. 19, 2010	391